Effect of Numerical Flame Resolution on the Acceleration History of a Premixed Hydrogen-Oxygen Flame Transitioning to Detonation

T. Alzer[1], J. Melguizo-Gavilanes[2], I. Wlokas[1], A. Kempf[1]
[1]Chair of Fluid Dynamics, EMPI, University of Duisburg-Essen, Duisburg, Germany
[2]Shell Global Solutions B.V., Major Hazards Management, Amsterdam, Netherlands

1 Introduction

Hydrogen is expected to play a key role in the future energy system, but its use poses significant safety challenges. A hydrogen-air mixture, such as one formed by leakage, has broad ignition and detonation limits. Among potential hazards, the deflagration-to-detonation transition (DDT) represents a worst-case scenario, where a subsonic deflagration rapidly evolves into a supersonic detonation, generating pressure spikes exceeding those of stable detonations. While DDT in obstructed channels is well-studied, this work focuses on its occurrence in smooth channels or pipes. Without obstacles, deflagration acceleration is influenced by complex physical phenomena, including burned-gas expansion, fresh-mixture compression, hydraulic resistance [1, 2], and turbulence interactions [3]. In smooth pipes, detonation onset may be triggered by interactions between the flame, boundary layer, and shocks. Due to its technical significance, DDT in smooth pipes has been widely investigated through experiments and simulations [4–9]. The review by Oran and Gamezo [10] provides a solid foundation on DDT mechanisms, while studies by Liberman et al. [11] and Ivanov et al. [12, 13] offer valuable 2D and 3D simulations of stoichiometric hydrogen-oxygen mixtures. Predicting the onset length and timing of DDT remains challenging, yet crucial for safety assessments. This work presents simulation strategies for predicting DDT in a smooth rectangular channel. Previous studies employed adaptive mesh refinement (AMR) and imposed symmetry constraints [14]. In contrast, we use a Cartesian, equidistant grid to reduce AMR-associated uncertainties and allow asymmetries to develop naturally. Simulation results are validated against experimental data from Ballossier et al. [9]. The report begins with an overview of the experimental setup, followed by descriptions of the numerical framework and simulation strategy. To assess the impact of flame resolution, results from non-thickened and thickened flame simulations at three refinement levels are compared. A time-space diagram illustrates detonation onset length, while simulated flame morphology is qualitatively evaluated against Schlieren measurements. Finally, the thermodynamic state at the flame tip prior to detonation is discussed.

2 Experimental Setup

In the experiment, an optically accessible channel of rectangular cross-section was filled with a stoichiometric H_2/O_2 mixture and ignited at the closed end of the channel. The channel was unobstructed,

Correspondence to: tom.alzer@uni-due.de

had smooth walls and a length of 1000 mm with cross-section dimensions of 9.4×10 mm. The channel was open to ambient conditions on one side. Schlieren measurements were taken in two orthogonal directions, allowing to reconstruct the spatial-temporal evolution of the flame tip. This setup allowed to fully characterize the flame acceleration dynamics and flame morphology, previously lacking in the literature. Their novel approach together with the simulation-friendly setup (the rectangular cross-section, moderate dimensions and the reported reproducibility) provides a solid baseline for developing a numerical model. A detailed description of the experimental setup and findings can be found in Ballossier's paper [8, 9].

3 Modeling and Numerical Methods

Simulations were performed using the compressible version of the in-house code PsiPhi [15, 16], developed at the Chair of Fluid Dynamics, Duisburg-Essen. PsiPhi solves the Favre-filtered Navier-Stokes equations on a Cartesian equidistant grid with efficient MPI-based parallelization. The system of equations describing the conservation of mass, momentum, energy and species can be found in the work by Lipkowicz [16]. A Riemann solver with Monotonicity-Preserving 5th-order reconstruction [17] is used for advective fluxes, while diffusive fluxes are handled via 2nd-order central differencing. Time integration follows a low-storage 3rd-order, 3-step Runge-Kutta scheme [18]. Combustion is modeled using finite-rate chemistry (FRC) within an operator-splitting framework [19], employing the Foundational Fuel Chemistry Model 1.0 (FFCM-1) [20]. To investigate the effect of flame resolution and reduce computational cost, an artificially thickened flame (ATF) approach [21] is used in selected cases. The ATF model is implemented by adjusting the transport coefficients in equations for energy and species conservation, as well as the source term in the equation for species conservation with a thickening factor F and efficiency function E. The thickening factor F is chosen to ensure the laminar flame structure at initial conditions is represented on 10 cells. The efficiency function E is computed according to the non-dynamic formulation and fit by Charlette et al. [21], where the sub-grid-scale turbulent velocity is computed from the turbulent viscosity of the LES sub-grid model. Turbulence is modeled within a Large-Eddy Simulation (LES) framework using the sigma model [22]. Thermodynamic properties of pure species are derived from NASA polynomials, while mixture properties are computed as mass-weighted averages. Molecular transport properties (viscosity, thermal conductivity, and binary diffusion coefficients) are determined from kinetic theory. The viscosity and thermal conductivity of the mixture follow the models of Wilke [23] and Mathur and Saxena [24], respectively. Species diffusion is treated using the mixture-averaged approach of Bird [25]. The numerical domain closely replicates the experimental setup, initialized with a stoichiometric H_2/O_2 mixture at 100 kPa and 298 K at rest. Ignition is achieved using a semi-spherical pocket of product gas (diameter 28–30% of the channel width) in equilibrium. Adiabatic, no-slip boundary conditions were applied throughout, except at the open end, where non-reflecting boundary conditions were used [26]. Two sets of simulations were conducted: one with ATF and one without. In both, grid resolution was varied by a factor of 2 per refinement step, ranging from 200 µm to 50 µm (six simulations in total). In the ATF cases, the static thickening factor ensured that a laminar flame propagating through the unburned mixture was resolved with 10 cells, meaning the artificial thickening decreased with increasing grid resolution. Simulations were run on AmplitUDE (ZIM, University of Duisburg-Essen) and SuperMUC-NG (LRZ, Munich). The highest-resolution case (397 million cells) utilized 3520 cores (AmplitUDE) and 76,800 cores (SuperMUC-NG).

4 Results and Discussion

Figure 1 presents the time-space evolution of the flame tip, with detonation onset marked by a sudden slope change in the t-x diagram. All simulations exhibit DDT, though the onset location and timing vary

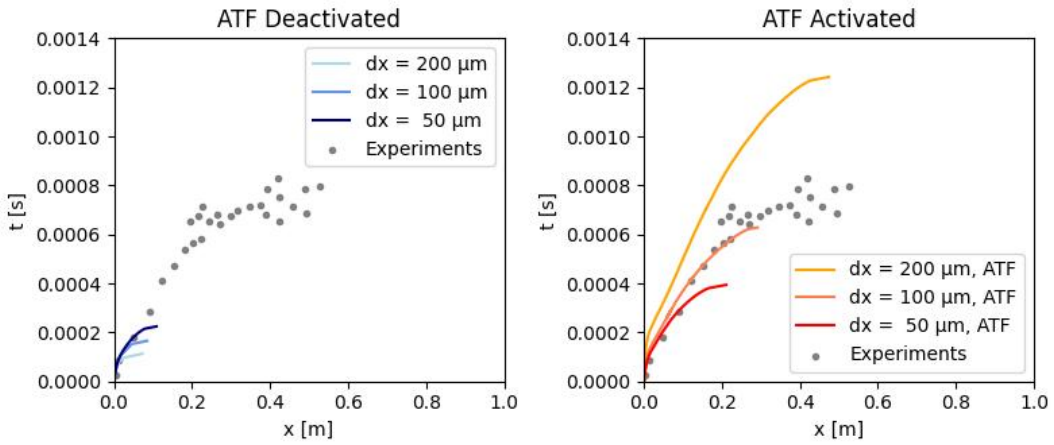

Figure 1: Time-space diagrams comparing results from simulations without (left) and with flame thickening (right) at three different grids to experimental results.

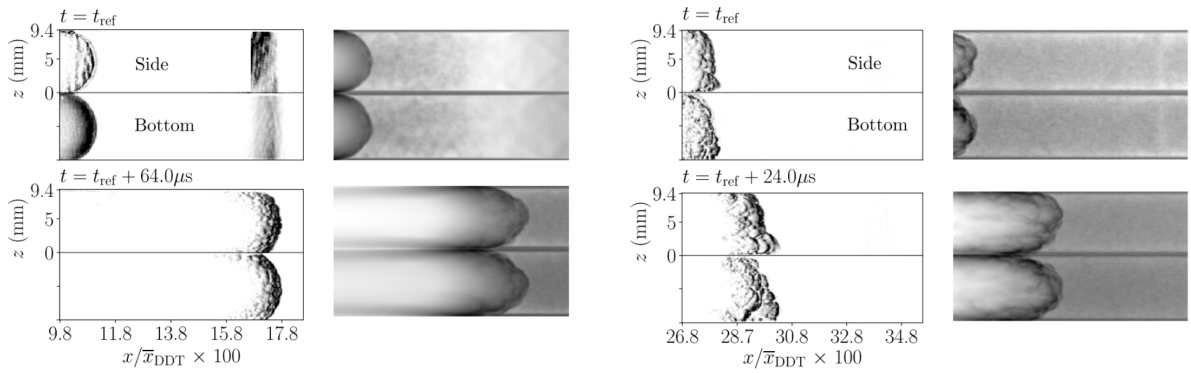

Figure 2: Qualitative comparison between experiment and simulation. Simulation results are from a simulation with activated ATF and on a medium grid of Δ=100 µm. The images from the simulation are taken at the same location as the experimental ones.

significantly with resolution and modeling strategy. Without flame thickening, detonation occurs far too early at all resolution levels. Increasing grid resolution delays flame acceleration and extends the onset length. In contrast, ATF drastically alters the results: on a coarse grid, detonation occurs too late, while on a medium grid, the onset time is close to the experimental data. However, on the fine grid, detonation happens too early again, as flame acceleration is overestimated. With ATF enabled, higher resolution leads to increased flame acceleration. Figures 2 and 3 provide a qualitative comparison of flame morphology, showing Schlieren images from experiments alongside numerical or pseudo-Schlieren images from simulations (ATF, 100 µm resolution). The key morphological features observed experimentally are reproduced in simulations: an initially smooth finger flame develops wrinkles, accelerates, and eventually transitions to detonation. Both in simulations and experiments, the flame tends to favor one side of the channel, a preference that increases with resolution. Experimentally, detonation typically initiates at the channel edges, a feature captured in the medium-grid simulation with ATF (Fig. 3). In other cases, detonation emerges from the flame tip, similar to simulations reported by Liberman et al. [11]. Figure 4 illustrates temperature and pressure fields shortly before detonation. The pressure rise ahead of the flame front reaches more than an order of magnitude above initial conditions, suggesting precompression effects. We suspect that insufficient resolution leads to numerical diffusion, artificially thickening the flame and overestimating heat release, thereby accelerating the transition to detonation.

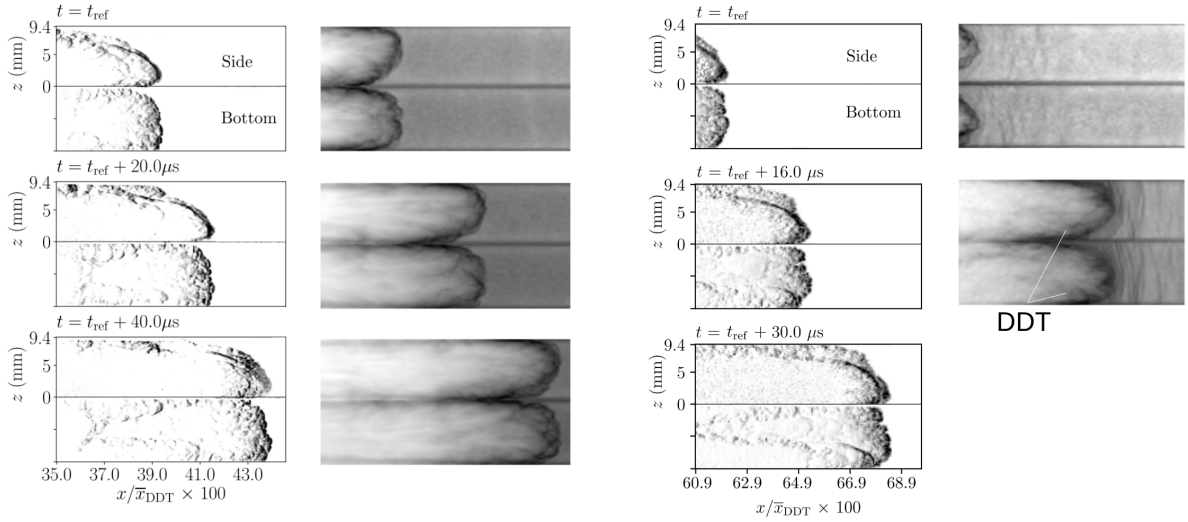

Figure 3: Qualitative comparison between experiment and simulation. Simulation results are from a simulation with activated ATF and on a medium grid of Δ=100 µm. The images from the simulation are taken at the same location as the experimental ones. DDT occurs in the last simulation snapshot.

This issue initially motivated the exploration of ATF, yet the current static thickening approach does not account for the flame thinning due to pre-compression (as seen in Fig. 4). One-dimensional laminar flame simulations indicate that at the elevated pressures observed in Fig. 4, the laminar flame thickness shrinks by a factor of 5 (from 0.24 mm to 0.05 mm). To improve DDT modeling, we propose refining the ATF strategy to dynamically adjust for changes in flame thickness and speed due to pre-compression. Additionally, wall modeling could enhance accuracy. Both approaches will be explored in future work.

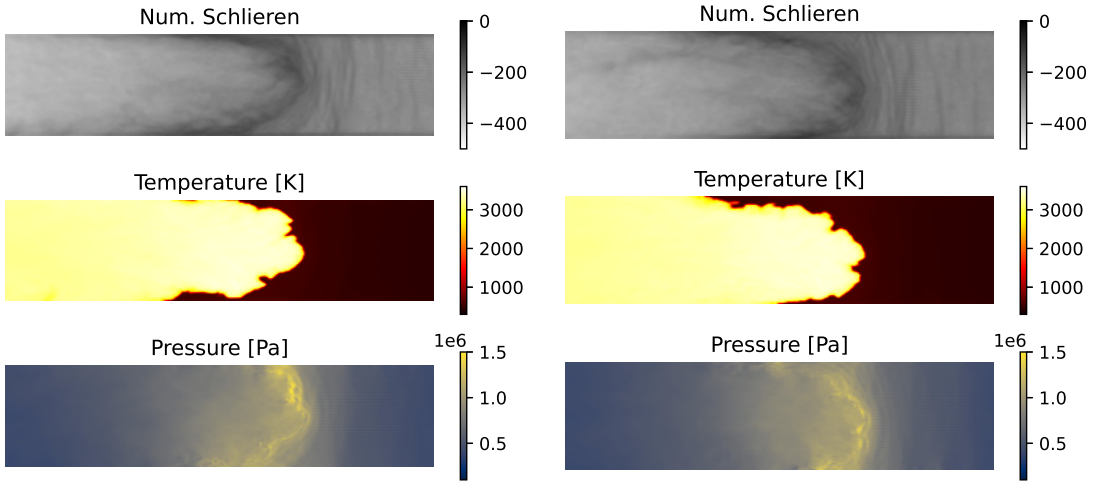

Figure 4: Details of the thermodynamic state prior to detonation onset. Shown are numerical Schlieren images and center planes of temperature and pressure.

5 Conclusions

The simulation results show a good agreement with the experimental observations of the flames morphology. The development of instabilities, the increase in distortion, and the tendency of the flame to

favor one side of the channel are all captured, although the latter is observed to a lesser degree in the simulations. The quantitative comparison of flame acceleration demonstrates that predicting the onset length and time of detonation remains difficult. The results for non-thickened flames significantly underestimate the onset length across all resolution levels. Introducing flame thickening improves agreement with the experimental range, shifting the predicted onset length closer to the measured values. With a time-step width that is dominated by convection, an n-fold refinement would lead to an n^4 times increase in computational cost. An n-fold increase of the flame-thickness by ATF, however, will not increase the cost at all. Despite this improvement, the thickened flame simulations do not fully converge on the experimental data. This remaining disagreement may be at least partly attributed to insufficient resolution of the flame structure toward the later stages of the simulation or the model mismatch if static ATF is applied. As the unreacted mixture becomes increasingly pre-compressed, the laminar flame thickness decreases, which may lead to under-resolution of the flame. However, it is not possible to clearly distinguish between numerical artefacts and physical model limitations at this point. Future work will focus on refining the modeling approach, particularly by developing an adaptive thickening strategy that accounts for variations in flame thickness and speed due to pre-compression effects.

Acknowledgements

The authors gratefully acknowledge the computing time granted by the Center for Computational Sciences and Simulation (CCSS) of the Universität of Duisburg-Essen and provided on the supercomputer amplitUDE (DFG project 459398823; grant ID INST 20876/423-1 FUGG) at the Zentrum für Informations- und Mediendienste (ZIM). The authors gratefully acknowledge the Gauss Centre for Supercomputing e.V. (www.gauss-centre.eu) for funding this project by providing computing time on the GCS Supercomputer SuperMUC-NG at Leibniz Supercomputing Centre (www.lrz.de).

References

[1] Brailovsky I, Sivashinsky GI. (2000). Hydraulic Resistance as a Mechanism for Deflagration-to-Detonation Transition. Combust. Flame 122:492-499.

[2] Kagan L, Sivashinsky G. (2003). The transition from deflagration to detonation in thin channels. Combust. Flame 134:389-397.

[3] Dorofeev SB. (2011). Flame acceleration and explosion safety applications. Proc. Combust. Inst. 33:2161-2175.

[4] Bykov V, Koksharov A, Kuznetsov M, Zhukov VP. (2022). Hydrogen-oxygen flame acceleration in narrow open ended channels. Combust. Flame 238:111913

[5] Kiverin A, Yarkov A, Yakovenko I. (2025). Explosion risks: Variety of deflagration-to-detonation transition scenarios in smooth tubes. Acta Astronaut. 226:325-331.

[6] Wieland C, Scharf F, Schildberg H-P, Hoferichter V, Eble J, Hirsch C, Sattelmayer T. (2021). Efficient simulation of flame acceleration and deflagration-to-detonation transition in smooth pipes. J. Loss Prev. Process Ind. 71:104504.

[7] Endo T, Kuwajima S, Kim W, Johzaki T, Shimokuri D, Miyoshi A, Namba SI. (2020). Deflagration-to-detonation transition in laser-ignited explosive gas contained in a smooth-wall tube. Combust. Flame, 219:275-282.

[8] Ballossier Y, Virot F, Melguizo-Gavilanes J. (2021). Strange wave formation and detonation onset in narrow channels. J. Loss Prev. Process Ind. 72:104535.

[9] Ballossier Y, Virot F, Melguizo-Gavilanes J. (2023). Flame acceleration and detonation onset in narrow channels: Simultaneous schlieren visualization. Combust. Flame 254:112833.

[10] Oran ES, Gamezo VN. (2007). Origins of the deflagration-to-detonation transition in gas-phase combustion. Combust. Flame 148:4-47.

[11] Liberman MA, Ivanov MF, Kiverin AD, Kuznetsov MS, Chukalovsky AA, Rakhimova TV. (2010). Deflagration-to-detonation transition in highly reactive combustible mixtures. Acta Astronaut. 67:688-701.

[12] Ivanov MF, Kiverin AD, Liberman MA. (2011). Flame acceleration and DDT of hydrogen-oxygen gaseous mixtures in channels with no-slip walls. Int. J. Hydrogen Energy 36:7714-7727.

[13] Ivanov MF, Kiverin AD, Yakovenko IS, Liberman MA. (2013). Hydrogen-oxygen flame acceleration and deflagration-to-detonation transition in three-dimensional rectangular channels with no-slip walls. Int. J. Hydrogen Energy 38:16427-16440.

[14] Houim RW, Ozgen A, Oran ES. (2016). The role of spontaneous waves in the deflagration-to-detonation transition in submillimetre channels. Combust. Theory Model. 20: 1068-1087.

[15] Lipkowicz JT, Wlokas I, Kempf AM. (2019). Analysis of mild ignition in a shock tube using a highly resolved 3D-LES and high-order shock-capturing schemes. Shock Waves 29:511-521.

[16] Lipkowicz JT, Nativel D, Cooper S, Wlokas I, Fikri M, Petersen E, Schulz C, Kempf AM. (2021). Numerical Investigation of Remote Ignition in Shock Tubes. Flow Turbul. Combust. 106:471-498.

[17] Suresh A, Huynh HT. (1997). Accurate Monotonicity-Preserving Schemes with Runge-Kutta Time Stepping. J. Comput. Phys. 136:83-99.

[18] Williamson JH. (1980). Low-Storage Runge-Kutta Schemes. J. Comput. Phys. 35: 48-56.

[19] Strang G. (1968). On the Construction and Comparison of Difference Schemes. SIAM J. Num. Anal. 5:506-517.

[20] Smith GP, Tao Y, Wang H. (2016). Foundational Fuel Chemistry Model Version 1.0 (FFCM-1), http://nanoenergy.stanford.edu/ffcm1

[21] Charlette F, Meneveau C, Veynante D. (2002). A Power-Law Flame Wrinkling Model for LES of Premixed Turbulent Combustion Part I: Non-Dynamic Formulation and Initial Tests. Combust. Flame 131:159-180.

[22] Nicoud F, Toda HB, Cabrit O, Bose S, Lee J. (2011). Using singular values to build a subgrid-scale model for large eddy simulations. Phys. Fluids 23:085106.

[23] Wilke CR. (1950). A viscosity equation for gas mixtures. J. Chem. Phys. 18:517-519.

[24] Mathur S, Saxena SC. (1967). Methods of calculating thermal conductivity of binary mixtures involving polyatomic gases. Appl. Sci. Res. 17:155-168.

[25] Bird RB. (2002). Transport phenomena. Appl. Mech. Rev. 55: R1-R4.

[26] Poinsot TJ, Lele SK. (1992). Boundary Conditions for Direct Simulations of Compressible Viscous Flows. J. Comp. Phys. 101:104-129.